A Practical Approach to Modeling Skin Effect in On-Chip Interconnects

Bhaskar Mukherjee
Dept. ECE
Stony Brook University
Stony Brook, NY 11794-2350
bmukher@ece.sunysb.edu

Lei Wang
Dept. ECE
Stony Brook University
Stony Brook, NY 11794-2350
leiwang@ece.sunysb.edu

Andrea Pacelli
Dept. ECE
Stony Brook University
Stony Brook, NY 11794-2350
pacelli@ece.sunysb.edu

ABSTRACT

A compact modeling methodology for the skin effect in conductors with rectangular cross section is presented. Possible equivalent circuit topologies are reviewed, and their calibration on numerical simulation is discussed, highlighting the shortcomings of conventional calibration procedures. A new approach, based on the direct fitting of the impedance transfer function to numerical simulations, is shown to offer excellent accuracy for a wide range of cross-sectional wire aspect ratios. The new formulation also obviates the need for separating the wire internal and external inductances which is a prerequisite for all published models. Finally, a practical implementation of the model as an *RL* parallel network is presented.

Categories and Subject Descriptors

B.7.2 [**Integrated Circuits**]: Design Aids

General Terms

Performance, design

Keywords

Interconnects, skin effect, circuit simulation

1. INTRODUCTION

High frequency interconnects for data and clock distribution and RF applications are a crucial component of all high performance electronic circuits. In recent years, increasing bandwidth requirements have led to research into low-loss on-chip interconnects, which theoretically can achieve very high bandwidth [1]. However, in the multi-gigahertz frequency range, skin effect causes current to flow only at the surface of conductors, leading to a decrease of wire inductance and an increase of resistance. The latter effect causes a signal attenuation which increases with frequency, thus limiting the available interconnect bandwidth.

Despite the technological impact of the skin effect, published models are mostly limited to traditional wire structures such as coaxial cables. For on-chip and on-board applications, it is important to be able to estimate the effect for single wires rather than complete transmission lines, and with a rectangular rather than circular cross-section. In particular, wires with high aspect ratios (width-to-height) are employed to reduce losses when the metal thickness is limited by technological considerations. Several numerical codes have been developed to compute current distributions in wires of any shape and arrangement [2, 3, 4, 5, 6]. Empirical fits of the frequency-domain wire resistance have also been presented [7], but their use in time-domain simulation requires an additional network realization step. To our knowledge, no general, efficient compact models exist in the literature for the important case of single wires with rectangular cross-section, which can be combined to model the skin effect for the overall layout.

In this paper we present a practical approach to the circuit modeling of skin effect in on-chip interconnects. Existing circuit topologies are reviewed and a new methodology for their calibration is presented. Three main modeling issues, not adequately addressed in previous works, can be identified. First, the total wire inductance must be decomposed into an *external* and an *internal* inductance, which are due to fields existing outside and inside the wire, respectively. As current crowds on the wire surface at high frequencies, the internal inductance vanishes. Second, the detailed dependence of resistance and inductance on frequency must be modeled by a transfer function with multiple zeros and poles (typically, two to four zero-pole pairs are used in the literature). Lastly, one must consider the problem of scaling the skin effect model with the wire length. It is well known that at low frequencies the inductance does not scale with length, because of the magnetic couplings along the length of the wire. However, the frequency dependence of the skin effect (and by extension also the internal inductance) should depend mainly on the wire cross-section and not on its length.

The work proceeds as follows. In Section 2 the published literature on skin effect modeling is briefly reviewed. The two main circuit topologies (*RL* ladder and parallel) are discussed, outlining the limitations of the conventional calibration procedure based on the arbitrary scaling of element values. Section 3 introduces a novel approach based on the direct replacement of the wire resistance by a rational transfer function. A simple parallel-*RL* implementation of this model is presented in Section 4. Finally, conclusions are drawn in Section 5.

2. EQUIVALENT CIRCUIT CALIBRATION

The skin effect can be represented at the circuit level as a combination of frequency-dependent resistance and inductance. However, frequency-dependent circuit elements are not suitable for time-domain analysis, therefore a circuit representation based on frequency-independent elements is desirable. All circuit models presented in the literature are based on the ladder topology of Fig. 1 or the parallel topology of Fig. 2. In both cases, the external inductance L_{ext} is frequency-independent, while the internal impe-

GLSVLSI'04, April 26–28, 2004, Boston, Massachusetts, USA.

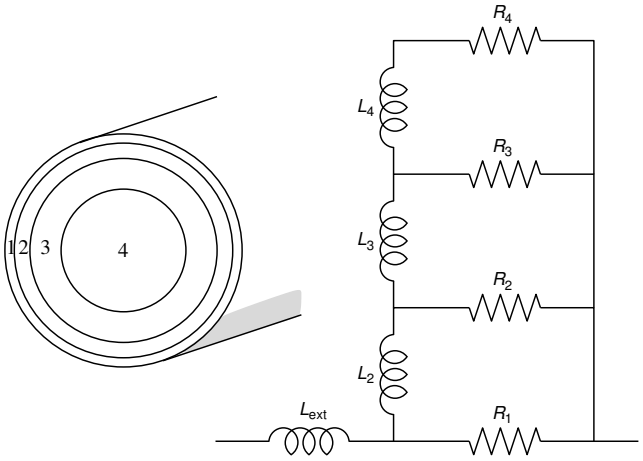

Figure 1: Ladder equivalent circuit for the skin effect and its physical interpretation for a wire with circular cross section. The wire is divided into four concentric regions, each with its own resistance $R_1 \cdots R_4$. Inductors $L_2 \cdots L_4$ progressively isolate the resistors from the current path, until at high frequency only resistor R_1 carries current. L_{ext} represents the external, or high frequency, inductance, which is not affected by skin effect.

dance (resistance and inductance) is modeled by a combination of resistors and inductors. The external inductance coincides with the asymptotic value of inductance at high frequencies,[1] and corresponds to the limit where all current flows on the wire surface and no fields exist inside the wire:

$$L_{\text{ext}} = L_{\text{hf}} \tag{1}$$

The internal inductance is the difference between the low- and high-frequency limits:

$$L_{\text{int}} = L_{\text{lf}} - L_{\text{hf}} \tag{2}$$

and is due to field penetration inside the conductor. Typically, internal inductance accounts for less than 10% of the total low-frequency (partial) inductance of a single wire, or open loop. For closely spaced loops, due to cancellation of the self- and mutual inductances, the internal inductance can be a significant portion of the loop inductance.

The ladder topology of Fig. 1 was introduced by Wheeler [8] and developed by Yen *et al.* [9] and Kim and Neikirk [10]. This topology can be rigorously justified from Maxwell's equations in the quasistatic limit, where each resistor R_i corresponds to a concentric shell in the physical conductor. Exact expressions for the inductances in the case of a circular cross section can be computed for a very fine discretization, i.e., a large number of thin shells [10]. However, no accurate expressions for the L_i's are known for a non-circular cross section, or a small number of shells. Kim and Neikirk developed a technique based on the ad-hoc assumption of a geometric progression of the resistance and inductance values [10]:

$$R_{i+1} = \frac{R_i}{RR} \qquad L_{i+1} = \frac{LL}{L_i}.$$

Once R_1 and L_2 are empirically set, the ratios RR and LL are chosen to satisfy constraints on the low frequency resistance R and internal

[1] Strictly speaking, the element L_{ext} in the parallel-RL circuit of Fig. 2 does not correspond to the high-frequency limit, however in practice it is very close to it.

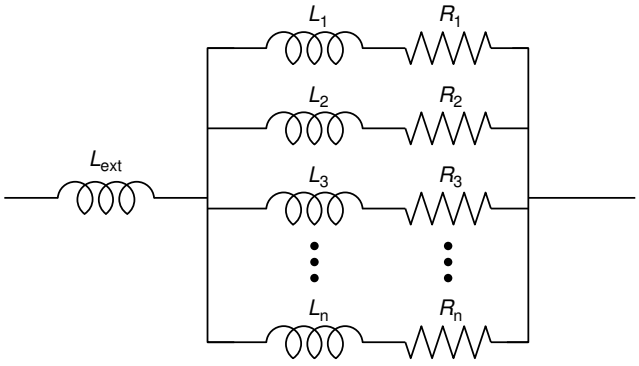

Figure 2: Parallel-RL model for the skin effect. Each of the R_iL_i pairs introduces a zero in the overall impedance. L_{ext} is the external inductance.

inductance L_{int}. The free parameters in the model are

$$\alpha_R = \frac{R_1}{R} \qquad \alpha_L = \frac{L_{\text{int}}}{L_2},$$

which are empirically fitted to exact analytical results or measurements. In [10], empirical rules were given to compute α_R and α_L based on wire radius and maximum frequency of operation. The fit was performed for a few representative cases, however no accounting for non-circular geometries was given. Also, no way was supplied to estimate L_{ext} and L_{int} except in special cases.

The parallel-RL topology (Fig. 2) has no direct physical interpretation, however due to its simplicity it is well suited for empirical fit of its parameters to measured data or exact theoretical results. Sen and Wheeler [11] supplied a set of rules to determine the parameters R_i and L_i for any number of parallel branches. Their derivation is similar to that of [10] in its being also based on the arbitrary assumption of geometric scaling of the resistors and inductors, and the conservation of R and L_{int}. Also in this case, no estimate was given for L_{ext} and L_{int}. Mei and Ismail [12] used the parallel-RL topology as a template for the model reduction of a complete, filament-based calculation. However the model generation requires extensive calculations, and no compact expressions are given.

In order to assess the efficacy of published models, we need to find a way to obtain the internal inductance of a wire for a given geometry, without relying on numerical solvers. However, the only formula readily available to estimate internal inductance is valid for a wire with circular cross section:

$$L_{\text{int}} = \frac{\mu l}{8\pi}. \tag{3}$$

Choudhury *et al.* have considered the internal inductance of a rectangular wire, however no expressions were provided for a generic aspect ratio [13]. We found that a satisfactory fit for a wire with width W and height H is given by the expression

$$L_{\text{int}} = 10^{-9} l[0.3 + 0.28\exp(-0.14W/H)] \tag{4}$$

where the wire length l is in centimeters, and where we assumed $W > H$ (the ratio H/W should be substituted for W/H in the opposite case). We have verified the accuracy of this expression by comparison with results obtained from FastHenry [3]. To ensure an accurate numerical modeling, a a 20×20 filament matrix was adopted in the FastHenry simulations. Note that FastHenry performs a magnetostatic calculation, where couplings along the wire length are

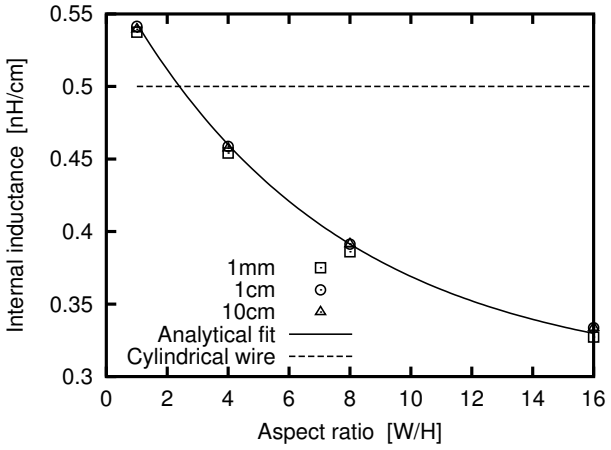

Figure 3: Symbols: Internal inductance per unit length, as obtained from numerical simulations using FastHenry, for three different wire lengths (1 mm, 1 cm, 10 cm). The numerical results show that the internal inductance scales with length and can be fitted by a single analytical expression (solid line). The value obtained for a cylindrical wire is also shown for reference (dashed line).

fully accounted for. On the other hand, expressions such as those of Eqs. (3) and (4) are per-unit-length quantities, and scale proportionally to length. Intuition suggests that, since the internal inductance depends on the cross-section of the wire, it should scale with length. This hypothesis is confirmed by Fig. 3, which compares the analytical expression to numerical simulations. The normalized internal inductance is essentially independent of length, but is strongly dependent on the wire aspect ratio. As explained in the next section, we will use this scalability to construct a model where all frequency-dependent quantities are independent of length. The figure also compares the analytical fit to the value of Eq. (3). For the examples of Fig. 4, Eq. (3) would suggest a value of internal inductance of 50 pH, which is in reasonable agreement only with the result obtained for a square cross-section.

Figure 4 shows the comparison between values of resistance and inductance obtained from FastHenry [3] and the model of Sen and Wheeler [11]. We considered the case of copper wires, of length 1 mm, with rectangular cross sections of constant area ($100\mu m^2$) and aspect ratios of 1, 4, and 16. As discussed above, the use of Eq. (4) allows a good fit of the inductance curve. However, the most dramatic consequence of the skin effect is not observed on the inductance, but on the resistance, which increases by over a factor of 10 from dc to 100 GHz. Since the wire geometry is not explicitly accounted for in the model, the qualitative dependence of resistance on the aspect ratio is captured only incidentally, and the quantitative match is not satisfactory, with errors exceeding 20%.

A similar result is obtained from the ladder model of Kim and Neikirk [10]. Also in this case, we used Eq. (4) to separate the internal from the external inductance. Since the original model was fitted on nonrectangular cross-sections, we recalibrated it from numerical simulations. Using least-squares optimization, we determined the parameters α_R and α_L for a wide range of aspect ratios. Fig. 5 shows the result of the fit for the same aspect ratios of Fig. 4. Also here, an error exceeding 20% is observed for the case $W/H = 16$. The slope of the $R(f)$ curve for high aspect ratios is quite lower than for the Kim-Neikirk model, and the best fit

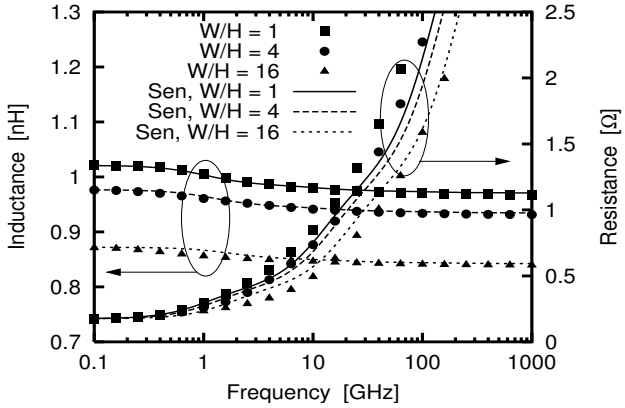

Figure 4: Comparison between FastHenry results (symbols) and the parallel-*RL* equivalent circuit of Sen and Wheeler [11] (lines). The equivalent circuit is based on the parallel *RL* structure of Fig. 2, with four *RL* branches.

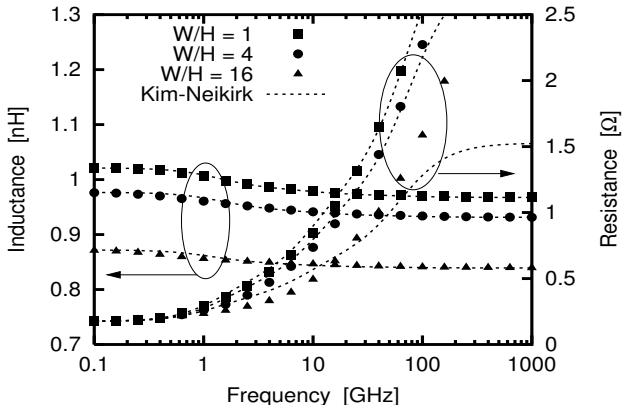

Figure 5: Comparison between FastHenry results (symbols) and the ladder model of Kim and Neikirk [10] (dashed lines). The equivalent circuit is based on the ladder *RL* structure of Fig. 1, with three *RL* branches. The model has been recalibrated by least-square optimization to supply a best fit to the numerical data.

crosses the numerical value rather than following it. Note the since an exhaustive optimization procedure was followed, no choice of model parameter exists that gives a better result. In fact, the assumption of fixed element scaling limits the representational power of the model. Moreover, the model parameters (α_R and α_L) do not have an immediate physical interpretation, and their scaling with the wire geometry is not obvious.

3. TRANSFER FUNCTION CALIBRATION

The results from the previously published models presented in Section 2 have shown their intrinsic limitations. These can be summarized as follows: (1) Lack of a model for L_{int}; (2) Failure to account for the wire aspect ratio; (3) Dependence on arbitrary scaling of resistor and inductor values. In this section we develop a direct approximation to the impedance transfer function, by placement of zeros and poles on the frequency axis. As a byproduct, we will automatically obtain the internal inductance as a function of the wire

resistance and the zero-pole frequencies.

In the new model, we write the total wire impedance as

$$Z = sL_{\text{ext}} + R\frac{(1+s/z_1)\cdots(1+s/z_n)}{(1+s/p_1)\cdots(1+s/p_n)} \tag{5}$$

where z_i and p_i are the zeros and poles of the resistive transfer function. Note that the entire frequency dependence is embedded in the resistive term. As opposed to the inductance-based models reviewed in the previous section, our model is resistance-based. By adopting this approach we can achieve better accuracy in the fitting of the frequency-dependent resistance, which is the main consequence of the skin effect, while obtaining the frequency-dependent inductance as a byproduct of the model.

In the low-frequency limit ($s \to 0$), Eq. (5) reduces to

$$Z \to sL_{\text{ext}} + R(1+s/z_1)\cdots(1+s/z_n)(1-s/p_1)\cdots(1-s/p_n)$$

$$\to s[L_{\text{ext}} + R\sum_i (1/z_i - 1/p_i)] + R.$$

From Eq. (2), we can then write

$$L_{\text{int}} = R\sum_i (1/z_i - 1/p_i). \tag{6}$$

This fundamental identity links the value of internal inductance to the frequency dependence of resistance. Moreover, due to its proportionality to the wire resistance, the internal inductance automatically scales with length, consistently with Eqs. (3) and (4). This allows us to keep the poles and zeros independent of wire length.

To complete the model, we performed an empirical fit of the zeros and poles to the numerical impedance curves for aspect ratios of 1, 4, and 16. We assumed that pairs of poles and zeros are equally spaced on the frequency axis:

$$z_2 = s_{zz} z_1 \qquad z_3 = s_{zz} z_2$$

$$p_1 = s_{zp} z_1 \qquad p_2 = s_{zp} z_2 \qquad p_3 = s_{zp} z_3$$

so that the only model parameters are the zero-pole spacing s_{zp}, the zero-zero spacing s_{zz}, and the frequency of the first zero z_1. From numerical optimization we obtained an excellent fit from the following values:

$$z_1 = \frac{2.2\times 10^{11}}{WH}\left(1 + 0.2[\ln(W/H)]^2\right) \tag{7}$$

$$s_{zz} = \frac{7.8}{(W/H)^{0.1}} \tag{8}$$

$$s_{zp} = 2.6\left(1 - 0.03[\ln(W/H)]^{3/2}\right) \tag{9}$$

where W and L are the wire width and height, in micrometers. Note that the above formulas assume $W > H$; In the opposite case one should replace H/W for W/H. Once the zeros and poles are generated, one obtains the internal inductance from Eq. (6). Figure 6 shows the fit of the zero-pole model to FastHenry results. Note that not only the dependence on the aspect ratio is reproduced, but no additional knowledge of the internal inductance is required, being replaced by Eq. (6).

We stress that these expressions are the result of an optimization process which was carried out for a given range of geometries, number of zero-pole pairs, and frequency range of interest. The process can be easily repeated for other situations and other sets of equations will be found. For example, we have performed the fitting trying to minimize the error on the resistance over the widest

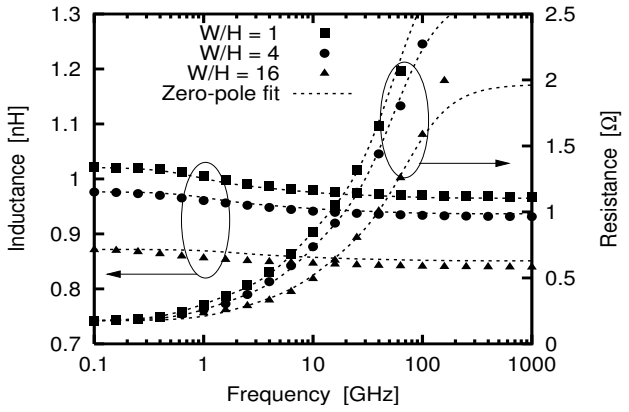

Figure 6: Comparison between FastHenry results (symbols) and the new model based on the direct zero-pole synthesis (dashed lines). Three zero-poles pairs were employed.

frequency range, while relaxing the inductance accuracy (which still remains within the order of 1%). A different optimization procedure, possibly employing a larger number of poles and zeros and/or a narrower frequency range, could result in a better accuracy on the inductance.

We finally observe that the values of zeros and poles of Eqs. (7)–(9) refer to copper wires. All results remain the same for other metals if one scales the first pole z_1 with the material resistivity:

$$z_1 = z_1^{\text{Cu}} \times \frac{\rho}{\rho^{\text{Cu}}}.$$

4. *RL* CIRCUIT IMPLEMENTATION

The direct zero-pole model can be introduced in any SPICE-like circuit, using controlled sources. For example, a simple high-pass circuit with one capacitor and two resistors can account for a single zero-pole pair where the zero frequency is lower than the pole's. An easier implementation can be approximated by the parallel-*RL* structure of Fig. 2. The impedance of this topology can be written as

$$Z = \frac{\prod_{i=1}^{n}(R_i + sL_i)}{\sum_{i=1}^{n}\prod_{j\neq i}(R_j + sL_j)} \tag{10}$$

therefore once the zeros and the resistances R_i are given, one can compute the inductances as

$$L_i = R_i/z_i.$$

The poles can be placed by operating on the resistor values, still within the constraint of conservation of the low frequency resistance:

$$R = \frac{1}{\sum_i 1/R_i}. \tag{11}$$

We pick a resistance scaling criterion similar to that of [11]:

$$R_{i+1} = s_R R_i$$

where s_R is a resistance scaling factor that we calibrate to the wire aspect ratio, essentially to try and replicate the overall zero-pole placement of Fig. 6 (as we did by varying s_{zp} in the direct pole-zero model). Once s_R is found, we can obtain R_1 from Eq. (11):

$$R_1 = R\sum_{i=0}^{n-1}(s_R^i)^{-1}.$$

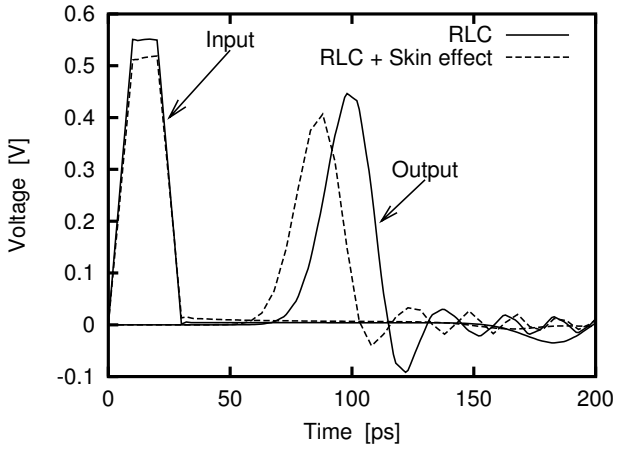

Figure 7: Impact of skin effect on high speed interconnect. The waveforms are shown at the input and output of a 1-cm differential transmission line. The copper conductors have a cross section of 40μm $\times 2.5\mu$m, and are separated by a 5μm gap filled with silicon dioxide.

Note that the transfer function of Eq. (10) has n zeros and $n-1$ poles, while our original approach assumed n zeros and n poles. Therefore we expect that in order to equal the accuracy of the zero-pole model of order n, we will have to employ $n+1$ branches of the parallel-*RL* topology. We obtained a good fit using the expression

$$s_R = \frac{3.6}{1+0.005(W/H-1)^{1.2}}$$

The result is completely analogous to that of Fig. 6 and is omitted for brevity. However, as mentioned above, it would be necessary to use four *RL* branches to equal the accuracy of the direct model with three zeros and three poles.

Having established the accuracy of the model, we can evaluate the practical impact of skin effect on interconnect performance. Figure 7 shows waveforms at the input and output of a 1 cm long differential transmission line, with cross-section 40μm $\times 2.5\mu$m and 5μm spacing. The conductor is copper ($\rho = 1.75\mu$Ohm-cm), while the insulator is silicon dioxide ($\varepsilon_r = 3.9$). A 1-volt, 20 ps pulse, with 10 ps rise and fall times, is transmitted from a matched driver to a matched load. All numerical simulations were performed using Hspice. The simulation shows that failure to account for the skin effect leads to three different errors. First, since the internal inductance is included in the line parameters, the line delay is overestimated. This error could be removed by including only the external inductance in the TL model, but this would underestimate the inductive effect at low frequencies. Second, the attenuation suffered by the signal due to line resistance is underestimated. Finally, the higher inductance leads to a higher characteristic impedance and incorrectly predicts loss of matching at the input (observed as a voltage higher than 0.5 V).

5. CONCLUSIONS

We presented a new calibration methodology for skin effect equivalent circuits, based on the fitting of the impedance transfer function to numerical simulations. The new model solves two problems intrinsic in previously published works, namely, the need for a separate expression for the internal inductance, and the failure to account for wires of generic cross-sectional aspect ratio. We showed that the methodology allows arbitrary accuracy in the modeling of the skin effect, and can be adapted to different situations and modeling requirements.

6. ACKNOWLEDGMENT

This work was supported by Defense Advanced Research Projects Agency (DARPA) and managed by the Sensors Directorate of the Air Force Research Laboratory, USAF, Wright-Patterson AFB, OH 45433-6543.

7. REFERENCES

[1] B. Kleveland, C. Diaz, D. Vook, L. Madden, T. Lee, and S. Wong, "Exploiting CMOS reverse interconnect scaling in multigigahertz amplifier and oscillator design," *IEEE J. Solid-state Circuits*, vol. 36, no. 10, pp. 1480–1488, Oct. 2001.

[2] W. T. Weeks, L. L. Wu, M. F. McAllister, and A. Singh, "Resistive and inductive skin effect in rectangular conductors," *IBM J. Res. Dev.*, vol. 23, no. 6, pp. 652–660, Nov. 1979.

[3] M. Kamon, M. Tsuk, and J. White, "FASTHENRY: A multipole accelerated 3-D inductance extraction program," *IEEE Trans. Microwave Theory and Techniques*, vol. 42, no. 9, pp. 1750–1758, Sept. 1994.

[4] G. Antonini, A. Orlandi, and C. R. Paul, "Internal impedance of conductors of rectangular cross section," *IEEE Trans. Microwave Theory and Techniques*, vol. 47, no. 7, pp. 979–985, July 1999.

[5] L. Daniel, A. Sangiovanni-Vincentelli, and J. White, "Proximity templates for modeling of skin and proximity effects on packages and high frequency interconnect," in *Proc. IEEE/ACM Intl. Conf. Computer Aided Design*, 2002, pp. 326–333.

[6] A. Rong, A. Cangellaris, and L. Dong, "A novel effective surface impedance formulation for efficient broadband modeling of lossy thick strip conductors," in *IEEE MTT-S Intl. Microwave Symposium Digest*, vol. 3, 2003, pp. 1959–1962.

[7] B. Kleveland, X. Qi, L. Madden, T. Furusawa, R. W. Dutton, M. A. Horowitz, and S. S. Wong, "High-frequency characterization of on-chip digital interconnects," *IEEE J. Solid-State Circuits*, vol. 37, no. 6, pp. 716–725, June 2002.

[8] H. A. Wheeler, "Formulas for the skin effect," *Proc. IRE*, vol. 30, pp. 412–424, Sept. 1942.

[9] C.-S. Yen, Z. Fazarinc, and R. L. Wheeler, "Time-domain skin-effect model for transient analysis of lossy transmission lines," *Proc. IEEE*, vol. 70, no. 7, pp. 750–757, July 1982.

[10] S. Kim and D. P. Neikirk, "Compact equivalent circuit model for the skin effect," in *IEEE Intl. Microwave Symposium Digest*, 1996, pp. 1815–1818.

[11] B. Sen and R. L. Wheeler, "Skin effects models for transmission line structures using generic SPICE circuit simulators," in *IEEE Topical Meeting on Electrical Performance of Electronic Packaging*, 1998, pp. 128–131.

[12] S. Mei and Y. I. Ismail, "Modeling skin effect with reduced decoupled $R-L$ circuits," in *Proc. Intl. Symp. on Circuit and Systems (ISCAS)*, 2003, pp. 588–591.

[13] J. Choudhury, G. S. Seetharaman, and G. H. Massiha, "Accurate modeling of thin-film inductance for nano-chip," in *Third IEEE Conference on Nanotechnology*, 2003, pp. 351–355.